Effect of dust particle size on the plasma characteristics in a radio frequency capacitively coupled silane plasma

Effect of dust particle size on the plasma characteristics in a radio frequency capacitively coupled silane plasma

Effect of dust particle size on plasma characteristics in a RF capacitively coupled silane plasma

Wen-Zhu Jia[1], Quan-Zhi Zhang[2], Xi-Feng Wang[1], Yuan-Hong Song[1]*, Ying-Ying Zhang[1] and You-Nian Wang[1]

[1]Key Laboratory of Materials Modification by Laser, Ion and Electron Beams (Ministry of Education), School of Physics, Dalian University of Technology, Dalian 116024, China

[2]Department of Chemistry, University of Antwerp, Campus Drie Eiken, Universiteitsplein 1, BE-2610 Wilrijk-Antwerp, Belgium

ABSTRACT

Compared with dust-free plasmas, existence of dust particles in plasmas may greatly influence plasma properties, such as the plasma density, electron temperature, sheath properties, electron energy distribution function (EEDF) as well as the heating mechanism. In this work, a 1D hybrid fluid/MC model has been developed to investigate the interaction between dust and plasma in a low-pressure silane discharge sustained in a radio frequency capacitively coupled plasma (RF CCP), in which we assume spherical dust particles with given radius are generated by taking the sum of production rate of $Si_2H_4^-$ and $Si_2H_5^-$ as the nucleation rate. From our simulation, the plasma may get definite perturbation by dust particles with certain radius (more than 50 nm), with an increase in electron temperature firstly, which further induces a rapid rise in the positive and negative ion densities. Then, the densities begin to decline due to the gradual lack of sufficient seed electrons. In addition, with the dust radius increasing, the high energy tails of EEDFs will be enhanced for discharge maintenance, accompanied by the decline in the population of low-energy electrons, in comparison with those of pristine plasma. Furthermore, an obvious bulk heating is observed apart from the α-mode and local field reversal heating. This may be contributed to the enhanced bulk electric field (also called the drift field) as a result of electron depletion via the dust. In addition, large sized dust particles that accumulate near the sheaths tend

to form two stable density peaks with their positions largely influenced by the time averaged sheath thickness. A detailed study of the effects of the external parameters including the pressure, voltage and frequency on the spatial distribution of dust particles is also conducted.

Key Words: dust particle; CCP discharge; electron heating mechanism; radio frequency;

* Corresponding author. Tel.: +86 0411-84707939; fax: +86 0411-84707939.

E-mail: songyh@dlut.edu.cn (Y-H Song).

1 INTRODUCTION

Dusty plasma is still a hot research topic due to rich variety of fundamental states and processes, such as wave propagation, mach cones, viscosity, phase transitions, lane formation, void and vortex, etc[1–8]. In semiconductor processing and tokamak fusion reactors, dust particles are usually considered as troubling problems which will cause plasma contamination and instability. Instead, they are indispensable in certain applications, such as manufacturing of nanomaterials and optimizing performances of thin films[9–12]. In low temperature plasmas, dust particles are considered to be produced either by homogeneous reactions in gas phase or by heterogeneous reactions during plasma–surface interactions[13]. Over the past decade, the detailed studies on chemical reaction pathways and possible precursors for particle formation in chemically active plasmas[14–26] have been conducted. Usually, most authors consider anion-neutral reactions in electronegative plasmas as the main pathway is responsible for the nanoparticle formation, due to long residence time of anions in the plasma compared with corresponding positive ions[20, 27, 28], although the role of neutral particles can not be completely excluded[29, 30].

Then, those particles formed by the gas-phase nucleation continue to grow by coagulation and condensation (i.e., rapid growth phase and growth saturation phase)[31–33]. Also, much attention had been paid to the dynamics and mechanism of the dust growth processes for a satisfactory description of the coagulation phenomena on the basis of various theoretical models. Kim[34], based on a gaussian distribution function of particle charges, analysed rapid particle growth processes caused by coagulation in a silane plasma reactor and compared well with the published experimental results by Shiratani[35]. Furthermore, they also discussed the changes in particle charge distribution during the rapid growth by the discrete-sectional model[36], and pointed that most of the large particles are charged negatively, while some fractions of small particles are in a neutral state or even charged positively. In addition, in order to explain a high cluster growth rate observed experimentally, Mankelevich[37] considered an additional attraction between the particles and introduced a polarization-induced ion flow asymmetry mechanism to the dust particle coagulation. Subsequently, Kim[38], using a modified collision frequency function between the nanoparticles in a coagulation module, investigated particle growth in an inductively coupled plasma. De

Bleecker[39, 40], by a 1D fluid model coupling with an aerosol dynamics model, in which charging of particles was taken into account based on the Orbital-Motion-Limited (OML) probe theory[41], showed that large particles during the dust growth tend to accumulate near sheath region with their density distribution like a bimodal structure, while small particles are inclined to stay in the discharge bulk. Warthesen[42], by self-consistently coupling a dusty argon plasma model with nanoparticle growth, charging, and transport models, concluded that the coagulation process is insignificant in a nanoparticle-plasma system, based on the results of the spatial distribution of dust particles in qualitatively good agreement with those in laser light scattering experiments[43]. Soon later, Ravi[44] further corrected the coagulation coefficients by introducing the effect of the image potential induced in neutral particles, and showed that coagulation is important for the growth of particles. Based on the above model, Agarwal[45, 46] studied the dust growth processes and revealed more detailed characteristics of dusty plasma, such as, the effects of nanoparticle size and charge distribution during the discharge.

In addition to understanding the growth mechanism and dust characteristics in the growth stage, at low temperature plasma, one of the most important aspects of dusty plasma research is to address the effects of dust on discharge properties, e.g., the electron energy distribution function (EEDF), electron heating mechanism, as well as the discharge stability. In general, in order to easily study the characteristics of dusty plasma, dust particles with a specific size and density might be injected directly into electropositive or electronegative plasmas, without considering the dust nucleation or growth processes[47, 48]. Actually, with the existence of dust in plasma, the electron density will decrease due to a large amount of electrons attached on the dust surface, accompanied by an increase in electron temperature because of an enhanced electron impact ionization compensating for the electron loss [49–56], which is well known as the enhanced intensity of the emitted light measured in experiments. However, some studies[57–59] also found that the change between electron density and temperature does not necessarily satisfy the above inverse relationship. For example, Killer[60], by using 160 GHz Gaussian beam microwave interferometry, found that when a large amount of large dust particles are added into a capacitively coupled RF argon plasma, a significant rise in the electron density is observed, which is considered to be due

to a surplus of highly energetic electrons created by more negative sheath potential in dusty plasma, contributing to an enhanced ionization rate[53]. In addition, Kushner[61] developed a Monte Carlo (MC) model coupled with a two-dimensional simulation to describe the effect of dust on glow discharges and implied that only when the density of dust is more than a certain value for a fixed pressure, can the plasma characteristics be affected.

Along with the plasma density and temperature, the EEDF is also influenced in a dusty plasma compared with a pristine discharge. Bilik[56], using a shielded Langmuir probe, experimentally investigated EEDFs in a capacitively coupled argon-silane RF plasma, and observed that as the population of lower energy electrons becomes less due to the existence of dust, the high energy tail in EEDF has a slight enhancement. At the same time, the EEDF changes from Maxwellian in pristine plasma to Druyvesteyn-like in the dusty plasma at 30 s after initiation, and then, transforms into Maxwellian distribution again at about 300 s. Deka[62] studied EEDFs for a magnetically filtered dusty plasma and illustrated that typical Druyvesteyn-like EEDF in pristine plasma may change to Maxwellian distribution at the presence of sufficient concentration of dust particles. In fact, in chemically reactive plasma containing dust, diagnostic tools such as Langmuir probe or electrostatic analyzer[56] are susceptible to contamination due to particle or film deposition on detectors, resulting in distortion of the current–voltage characteristics, so experimental measurements still lack in dusty plasma. Most understanding about the evolution of EEDFs in dusty plasmas still relies largely on numerical simulation. By using a Monte Carlo/fluid hybrid model, Kushner[61]pointed out that the amount of high-energy electrons in the EEDF will decrease at the presence of dust particles at fixed electric field. Goedheer[63] introduced a 1D PIC/MC model to investigate a capacitively coupled silane/hydrogen plasma and indicated that when going from large amount of small particles into small amount of large particles, a higher energy tail of EEDF would appear. Moreover, properties of a capacitively coupled rf discharge sustained in argon and in a mixture of Ar/C_2H_2 with nano-size particles had been studied by employing particle-in-cell dust models[64], assuming a constant dust density. From this work, it was found that, for Ar plasma without dust, the EEDF follows Maxwellian distribution, while typical Druyvesteyn like EEDFs are observed in Ar/C_2H_2 dusty plasma, with their density distributions of dust in agreement with the corresponding

experimental results[65].

Another important issue is about the electron heating mechanism in RF CCPs. As well known, there are two common heating modes, i.e., α-mode and γ-mode, characterized by outstanding ionization/excitation maxima near the sheath edge due to sheath oscillation, or maintained by secondary electrons from wall surface. However, in electronegative plasmas, there is an additional bulk heating mode (i.e. drift electric field heating) observed[66–71], which is considered to be due to enhanced drift electric field caused by low electrical conductivity. In addition, a so-called drift-ambipolar heating mode (DA mode)[72] in strongly electronegative CF_4 plasmas has driven much attention, characterized by obvious ionization/excitation in the bulk and at the sheath edges, caused by strong drift and ambipolar electric fields. Furthermore, another heating mode during the sheath collapse is caused by field reversals[73, 74]. The reversed field appears, to accelerate electrons hindered by collisions to balance the ion flux to the electrodes. Thus, field reversals will be affected by the gas pressure and mobile ions.

When dust appears and becomes sufficient to affect the discharge properties, changes in heating mechanism in RF CCPs would inevitably occur. A transition from low-pressure, low-voltage regime (α-mode) to high-pressure, high-voltage regime (drift electric field mode) has been observed in a silane discharge by optical and electrical measurements[75]. And then, based on both fluid and particle-in-cell models, Boeuf[76] had inferred this mode transition attributed to the increase in the electron loss rate during the dust formation. Schungel[55], by phase-resolved optical emission spectroscopy (PROES), reported that a hybrid combination of α-mode and the local field reversal heating in pure H_2 discharge would transform into just a drift electric field mode in hydrogen diluted silane discharges, due to loss of a large amount of electrons by dust particles. Subsequently, by adding dust particles with specified size, density, and uniform spatial distribution into argon plasma, a drift electric field mode was observed for the first time in the electropositive plasma[54]. However, in terms of numerical simulation, detailed studies on the relationship between dust and heating mechanism in electronegativity plasmas are still expected, especially for the impact of the dust existence on the field reversal heating and drift electric field mode.

Based on the above analysis, on the one hand, we will study the effect of dust on the heat-

ing mechanism, plasma density, electron temperature and EEDF in a capacitively-coupled RF silane discharge. On the other hand, we also try to figure our the effects of discharge parameters on the spatial distribution of dust. This paper is organized as follows. The model is briefly described in section 2 and our results are discussed in section 3. Some concluding remarks are present in section 4.

2 DESCRIPTION OF MODEL

A one-dimensional fluid/MC simulation is adopted in this work, in which the EEDFs are acquired by using an electron Monte Carlo simulation (eMC). Usually, fluid modeling is a good choice for simulation of plasma transport processes with complicated chemical reactions, since it has a lower calculation cost compared with that of the PIC model. Detailed descriptions of fluid model can be found in literatures[40, 77], in which density and its momentum balance equations, coupled with Poisson's equation are involved. For electron, ions, neutrals and dust particles, their densities are described by the particle balance equations. The fluxes of electron and ions are determined by the drift-diffusion approximation, with the inertia effects of ions considered by introducing an effective electric field[77] instead of the instantaneous electric field. Since neutral particles are not affected by the electric field, the corresponding flux includes only the diffusion term. The electric field in the plasma is calculated by the Poisson's equation. And then, ions, neutrals and dust particles are assumed at room temperature, while the electron temperature can be derived from the integration of EEDFs by eMC approach[78]. In eMC, collisions with the background gas and dust particles are carried out, including elastic scattering, ionization, excitation of molecules and absorption on the dust surface, in which the corresponding cross section of electron with dust particles can be approximated [54, 79], based on the ideal Orbital Motion Limited (OML) theory[80], as

$$\sigma_{ed} = \pi r_d^2 (1 + e\varphi_{fl}/\varepsilon_e), \text{ for } \varepsilon_e \geq -e\varphi_{fl}, \tag{1}$$

$$\sigma_{ed} = 0, \text{ for } \varepsilon_e < -e\varphi_{fl}, \tag{2}$$

where r_d, e, φ_{fl}, and ε_e denote the dust radius, elementary charge, dust floating potential, and electron kinetic energy, respectively. If the electron energy is less than the floating potential energy, electrons cannot reach the dust surface, and then the collision cross section is set to 0. The other cross sections in SiH_4 are taken from Refs.[39]. When the EEDF is obtained from eMC, the electron transport coefficients and electron-impact source terms can be returned to the fluid model. Furthermore, the resulting electric field and related particle density distribution calculated from the fluid model will be transferred to the next run of eMC. These two processes advance iteratively over time until the plasma reaches a steady state.

The charging of the dust can be described by

$$\frac{dQ_d}{dt} = I_e + I_i, \tag{3}$$

where Q_d, I_e and I_i are the dust charge, the electron and ion current towards the dust surface, respectively. Note that the charging of dust does not include the contribution of negative ion current, because the negative ions are considered to have no sufficient kinetic energy to overcome the potential barrier of the dust, in the discharge condition in this work. The electron and ion current can be obtained from the OML theory[20]. According to the expression $Q_d = 4\pi r_d \varphi_{fl}$, the dust floating potential can be also obtained. As we know, since the charging time is in the order of microseconds[81] which is more than the RF period (i.e, tens of nanoseconds), but less than the growth time of dust (about the order of seconds)[82], the floating potential of the dust particle in the simulation process is assumed to be constant during one rf cycle, and is quickly established as soon as the dust is formed in plasma. These simplifications can effectively save the computation cost.

The dust transport is determined by several different forces including the electric field force, gravitational force, thermophoretic force, as well as the ion and neutral drag force. The electric field force will compel the negatively charged dust away from the electrodes. The gravitational force is not important for sub-micrometer particles[83], thus we ignore it in the model. The thermophoretic force caused by the temperature gradient in the background gas is not considered in our model either, since the background gas temperature is assumed to be constant. The ion drag, exerted on dust nanoparticles by positive ions moving from

the discharge center toward the walls, is believed to be likely responsible for the formation of dusty voids, with the collection (F_i^c) and orbit (F_i^o) components considered [40], given as

$$F_i = F_i^o + F_i^c = (4\pi b_{\pi/2}^2 \Gamma + \pi b_c^2) m_i v_s \Gamma_i = \chi \Gamma_i, \tag{4}$$

where Γ_i is the ion flux and $\Gamma = \frac{1}{2}\ln(\frac{\lambda_{De}^2 + b_{\pi/2}^2}{b_c^2 + b_{\pi/2}^2})$ is Coulomb logarithm dependent on the electron Debye length λ_{De}. And, $b_c = r_d\sqrt{1 - \frac{2e\varphi_{fl}}{m_i v_s^2}}$ stands for the collection parameter, while $b_{\pi/2} = r_d\sqrt{\frac{e\varphi_{fl}}{m_i v_s^2}}$ is the impact parameter in the case of the deflection angle $\pi/2$, $v_s = (\frac{8k_B T_{gas}}{\pi m_i} + v_i^2)^{0.5}$ is the ion mean velocity, m_i is the ion mass and v_i is the ion velocity. In addition, the expression $(4\pi b_{\pi/2}^2 \Gamma + \pi b_c^2) m_i v_s$ is marked as χ for the convenience of the following discussion. Also, we have noted that an improved model for ion drag force had been proposed by Khrapak while considering large angle scattering processes [89]. However, according to Land [90], for dust particles below the micrometer regime, results from the current model can be much closer to those based on Khrapak theory.

Assuming the neutral drag force always balances the sum of the other forces, a drift–diffusion like equation can be obtained for the dust, as

$$\Gamma_d = -\mu_d n_d E_{eff} - D_d \frac{dn_d}{dx} + \sum \frac{n_d}{m_d \nu_{md}} \chi \Gamma_i, \tag{5}$$

where $m_d, n_d, \mu_d = Q_d/m_d\nu_{md}$ and $D_d = \mu_d k_B T_{gas}/Q_d$ are the reduced mass between dust and background gas, dust density, nanoparticle's mobility and diffusion coefficients, respectively. And, $\nu_{md} = \sqrt{2}\frac{P_{tot}}{k_B T_{gas}} \pi r_d^2 \sqrt{\frac{8k_B T_{gas}}{\pi m_d}}$ is the momentum loss frequency where P_{tot} is the pressure and k_B *is* Boltzmann constant.

In this model, the gas phase chemical reactions are adopted from De Bleecker's work[39], in which, anion-neutral reactions are considered to be the main pathway for the nanoparticle formation. Actually, our research is intended to focus on the effect of the dust existence on the plasma properties, rather than the dust growth path. Thus in our model, the particles with a given radius are assumed to be formed at the production rate of the anions. We adopt the sum of the production rate of $Si_2H_4^-$ and $Si_2H_5^-$ as the source term of dust in order to reduce the cost of computing time. It should be noted that the generation of dust particles is essentially similar to the injection of dust particles into the plasma at a constant rate. This simplification does not affect our research focus. On the other hand, the dust particle

size is considered to be approximately monodisperse (i.e. all the dust have a uniform size). In addition, we take into account the recombinations of positive ions on the dust particle's surface, by means of a recombination rate[77] which is considered as a very important loss path for positive ions in the plasma.

The model is solved as follows. By using the hybrid model, the plasma is first calculated and achieves a steady state solution after about 20,000 RF cycles (.i.e., 0.4 ms), without dust in the plasma. Then dust is introduced in the plasma with a non-zero nucleation rate, and a two-step method[77] is used to treat the nanoparticle versus plasma dynamics. First, plasma equations are solved with a small time step over several cycles as the nanoparticles remain stationary. Second, the nanoparticle transport and charging calculations are executed with a greater time step basing on time averaged plasma properties. However the nanoparticle charging will cause an excess space charge region and result in instabilities in solving the Poisson's equation when running the first step again. To overcome this numerical instability, we adopt the method proposed by Akdim[77] in which the excess space charge caused by dust is corrected by self-consistently adapting the positive ion density distributions before running the first step. At last, a steady state for plasma will be achieved again. The discussion given below shown in this work is all based on this steady results after calculating 60,000 RF cycles.

3 RESULTS AND DISCUSSION

In this section, by combining a hybrid fluid/MC model with a dust transport model, we study the influence of dust size on the plasma properties and the effect of the discharge parameters on the dust distribution. The base operating conditions are the gas temperature of 400 K, radio-frequency of 50 MHz connected to the lower electrode, RF voltage amplitude of 100 V, pressure of 300 mTorr (40 Pa) and electrode spacing of 3 cm. Under such typical operating conditions, dust particles would be easily formed[84]. The density of small sized dust with the diameter of 1 and 2 nm ranges from 10^8 cm^{-3} to 10^9 cm^{-3} or even lower in the corresponding experiment[85], and becomes much lower as the radius of the dust increases. Thus, we assume in our simulation that, once the maximum density of dust reaches 10^8 cm^{-3}, the formation of dust will be terminated.

3.1 The effect of radius of dust particle on the plasma properties

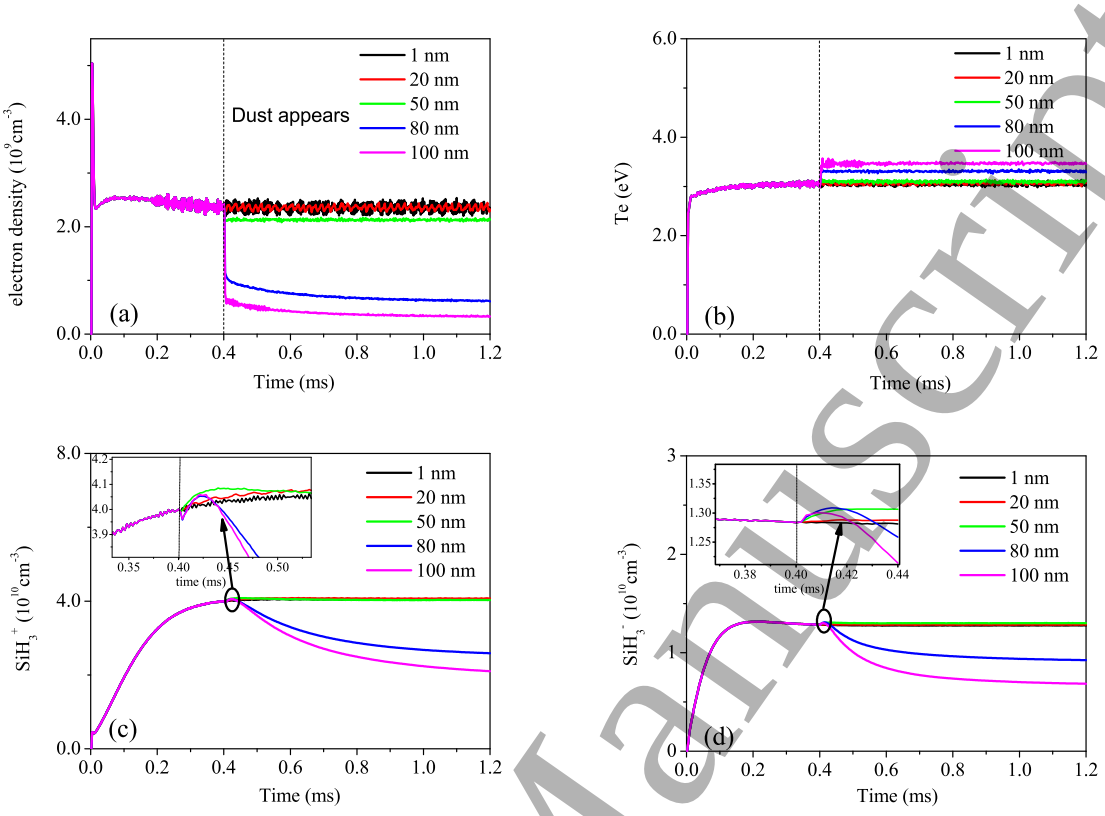

Figure 1. Time evolutions of electron density (a), electron temperature (b), positive ion density (SiH_3^+) (c) and negative ion density(SiH_3^-)(d) at the discharge center for different dust radii, where dust appears at 20000 RF cycles, i.e., 0.4 ms. The base discharge conditions in pure silane are operated at radio-frequency of 50 MHz, RF voltage amplitude of 100 V, pressure of 300 mTorr (40 Pa) and electrode spacing of 3 cm.

Figure 1 shows time evolutions of the electron density, electron temperature, positive ion density (SiH_3^+) and negative ion density (SiH_3^-) at the center of discharge with the existence of different radii of dust particle. As can be seen clearly that, for the existence of smaller sized dust particles($\leq$20 nm), almost no change can be observed in the plasma properties. However, as the radius of dust particle increases to be greater than 50 nm, the electron density decreases evidently, which can be attributed to the electron collection by the dust. Meanwhile, the electron temperature increases, as shown in figure 1(b). This result supports the current main conclusion about the inverse relationship between the electron density

and temperature in dusty plasma[49–56]. Furthermore, the time evolutions of positive and negative ion densities in dusty plasma are shown in figure 1(c) and (d). It is noticed that, for the cases of larger sized dust particles ($\geq$50 nm), there are evident overshoots (as shown in the illustration) in both the positive and negative ion density profiles, before the densities attain their steady states. We think that this transient rise is as a result of an increase in the relevant source term caused by the rapid increase in electron temperature. The subsequent decrease in the positive ion density is, on the one hand, due to the recombination loss at the dust surface, and on the other hand, due to the lower electron density which would result in the weakening of the generation source in corresponding chemical reactions. Furthermore, the decrease in the density of SiH_3^- is only attributed to the second reason (the lower electron density), because the charging effect of negative ions on dust, as well as loss mechanism of SiH_3^- directly for dust particle formation, is not considered in the simulation.

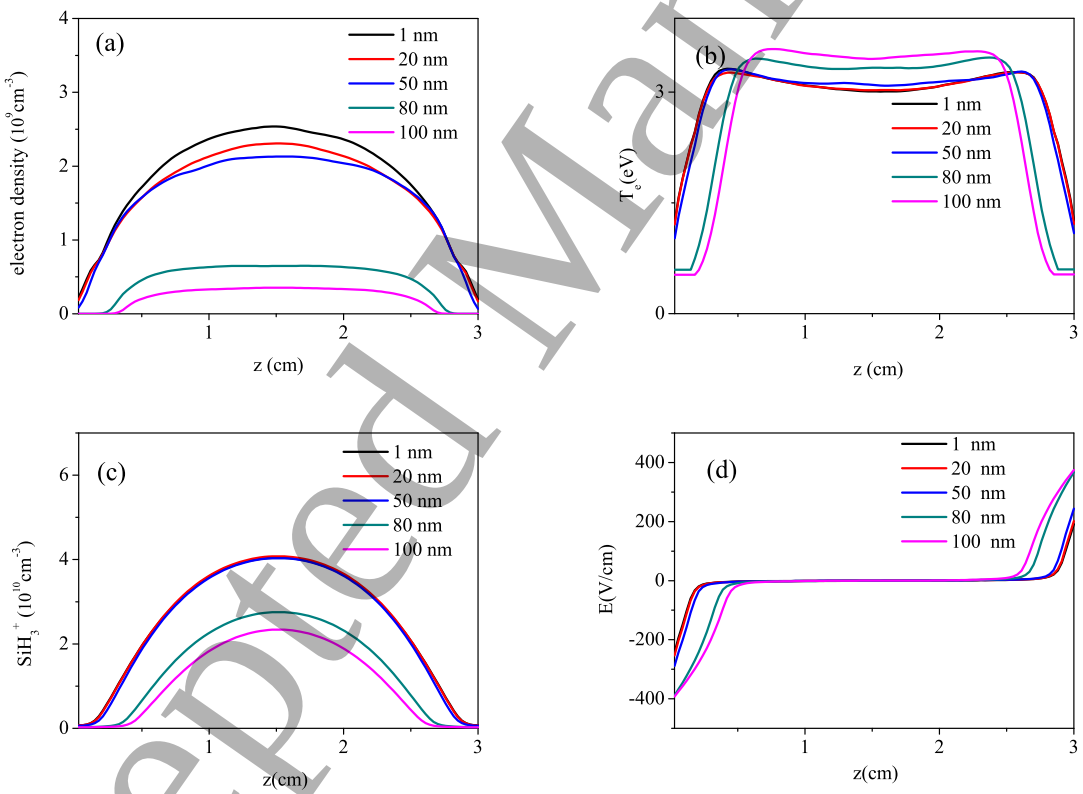

Figure 2. Spatial distributions of time averaged electron density, electron temperature, positive ion density and electric field for different dust radii. The discharge conditions are same as in figure 1.

Figure 2 exhibits the spatial distributions of time averaged electron density, electron temperature, positive ion density and electric field. As the radius of dust particle increases to more than 80 nm, the plasma density in the bulk decreases definitely, leading to the increase of the sheath thickness which can be observed from the density and electric field distributions, in agreement with the results of Akdim[77]. It should be noticed that the sheath thickness discussed in this paper generally refers to the averaged one over one RF cycle. Moreover, in the bulk, the electron temperature gradually increases with the radius of dust particle increasing, though no special changes in the profiles of the electric field are observed in this figure. Actually, the effect of dust size on the temporal electric field in the bulk exists and could lead to a transition of the electron heating mechanism, which will be discussed in the next part. In addition, it is predictable that with more larger sized particles added, the discharge might inevitably quench, since few seed electrons would be left for ionization. Besides, serious instability of discharge may occur, such as the emergence of arc discharge[61].

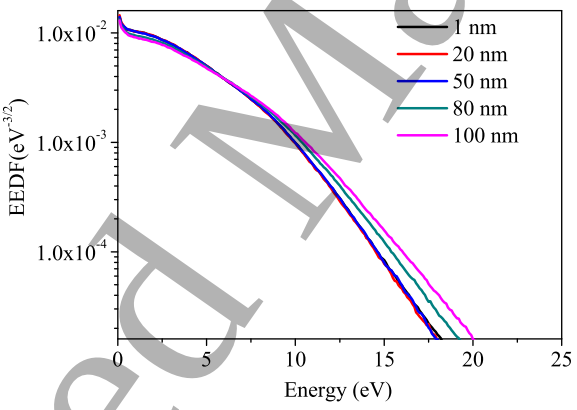

Figure 3. Time-averaged electron energy distribution functions averaged over the plasma for dust radius of 1 nm, 20 nm, 50 nm, 80 nm and 100 nm. The discharge conditions are same as in figure 1.

The electron temperature reflects the macroscopic characteristics, while the EEDF can embody the microscopic characteristics of electrons in the plasma. Figure 3 shows the time and space averaged EEDF for different radii of dust particle. It can be seen that when the radius of dust particle changes from 1 nm to 50 nm, there is no obvious variation on the

EEDF, similar to that in dust-free situation. However, when the radius of dust particle reaches 80 nm (or even greater), the population of low energy electrons declines owing to dust surface collection, accompanied by an increase in a number of high-energy electrons, which suggests a significant increase in the electron temperature (see figure 2 above). More high-energy electrons are attributed to the ionization enhancement as compensation for the loss of electrons. And we notice that all the EEDFs show Druyvesteyn like distribution, in agreement with the results given by PIC simulation in pure silane[68]. These EEDFs indicate that the plasma is in a non-equilibrium state.

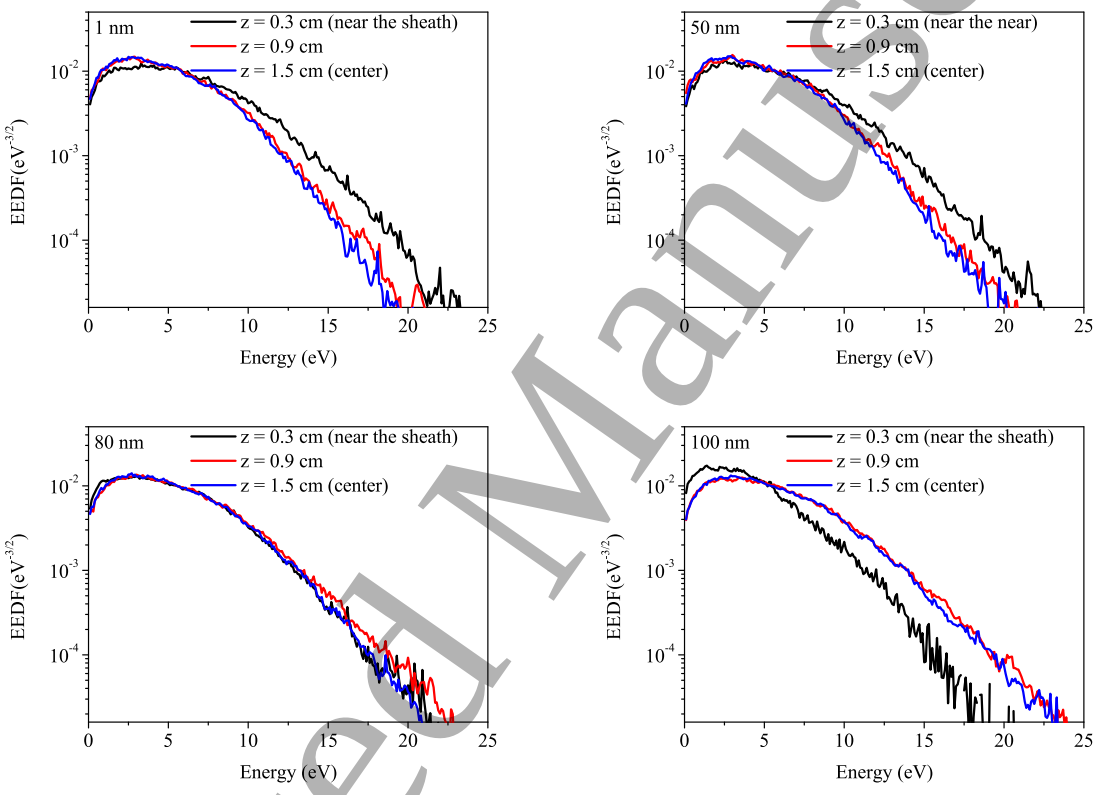

Figure 4. Time-averaged electron energy distribution functions at different positions (z = 0.3 cm, 0.9 cm and 1.5 cm) for dust radius of 1 nm, 20 nm, 50 nm, 80 nm and 100 nm. The discharge conditions are same as in figure 1.

In addition, we also show the time averaged EEDFs at $z = 0.3$ cm (near the sheath), $z = 0.9$ cm, and $z = 1.5$ cm (center of the discharge), with different radii of dust particle in figure 4. For the case of smaller dust particles (≤ 50 nm), more high energy electrons near the sheath ($z = 0.3$ cm) are observed than those in the bulk ($z = 0.9$ and 1.5 cm), due to

acceleration of electrons by the expanding sheath. As the dust particle radius increases and the disturbance to the plasma becomes more obvious, the sheath thickness becomes larger, so that the position $z = 0.3$ cm selected here may locate in the sheath area as shown in figure 2, resulting in a change from 22 eV to 20 eV in the high-energy tail of EEDF. However, the high-energy tail of EEDF at $z = 1.5$ cm gradually enhances from approximately 20 eV to 25 eV as the radius of dust particle is large enough. This not only explains the tendency of the electron temperature at fixed locations (such as $z = 0.3$ cm, $z = 1.5$ cm) with increasing radius of dust particle in figure 2, but also suggests transition of electron heating mode.

3.2 Heating mechanism in dusty plasma

The heating mechanism is a crucial parameter for plasma, and can be largely affected by the presence of dust particles. We thus present the spatiotemporal profiles of the electron impact source term (the term on the right hand side of the electron continuity equation which represents sum of the source and loss terms for electron production) (first column), as well as the electric field (second column) in figure 5 under the base discharge conditions for different sizes of dust particle. Generally, for the case of 1 nm, two electron heating mechanisms dominate. One is called the typical α-mode heating, in which electrons are accelerated with the enhanced electron impact source term during the sheath expansion phase as shown in figure 5(a). The other is the reversed field heating mode caused by the field reversal near the collapsing sheath. As the sheath collapses, the positive ions in the sheath are gradually exposed, while the electrons near the sheath cannot timely shield them, due to the collision processes. As a result, separate charges will cause the occurrence of a reversed electric field in the opposite direction of the applied electric field. This field reversal, as shown in figure 5(b) (labeled '1'), will accelerate the electrons to ensure the quasineutral and cause a maximum electron impact source term near the collapsing sheath in figure 5(a) (labeled '1'). Therefore, it can be inferred that if the electrons are hindered, a strong field reversal will appear in the sheath collapse region.

Moreover, when increasing the dust particle radius to 80 nm in plasma, a bulk heating effect maintained by the drift field is observed obviously, as shown in figure 5(c) and 5(d). Since the significant loss of electrons by the attachment on the dust surface would induce a

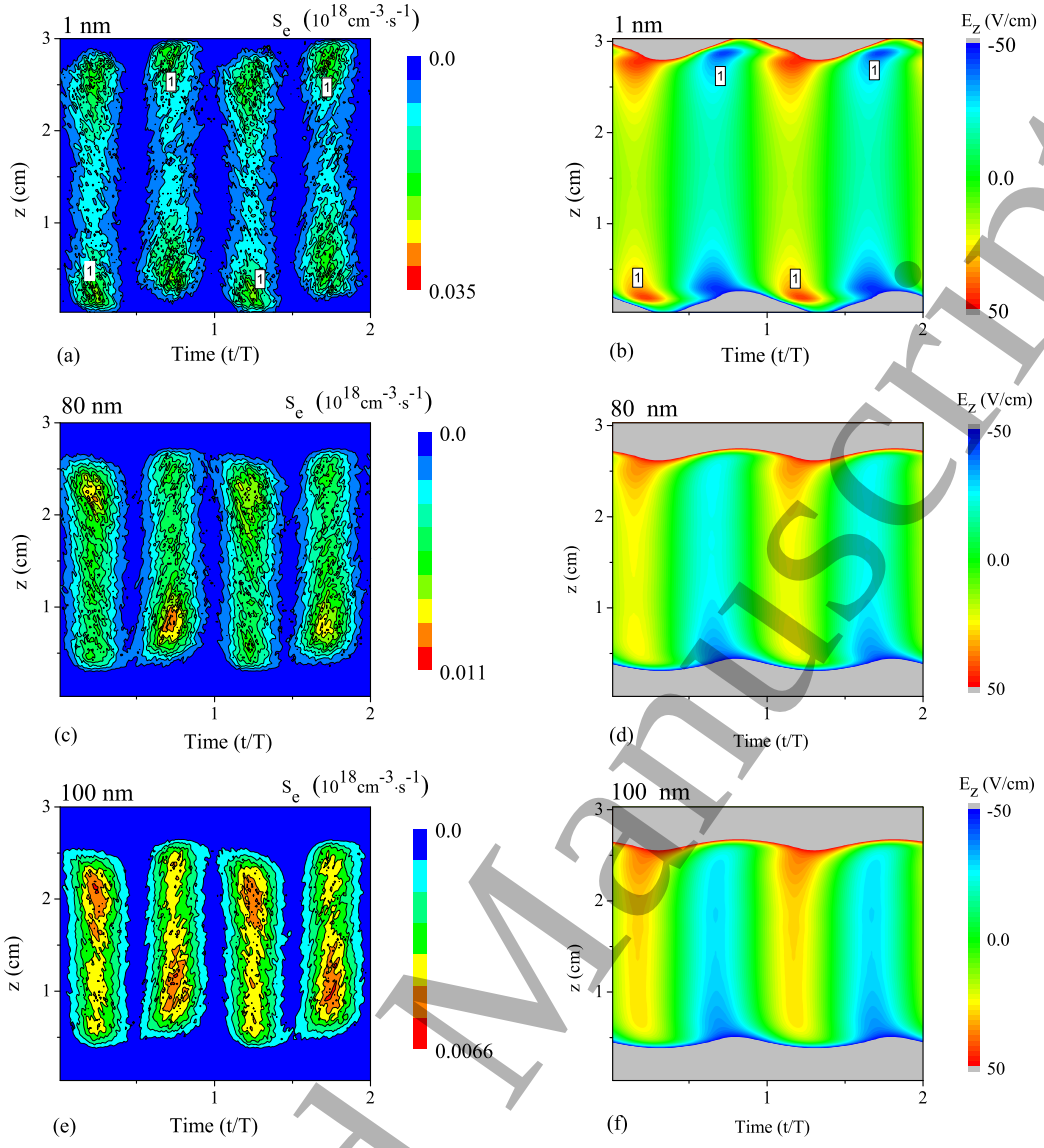

Figure 5. Spatiotemporal evolutions of electron impact source term(first column), corresponding electric field (second column) during two rf cycles in SiH_4 discharges driven by 50 MHz, for dust radius of 1 nm (first row), 80 nm (second row), 100 nm (third row) present in the plasma. The electric field reversal and its heating mode are labeled '1' in the graphs. The discharge conditions are same as in figure 1

decreased plasma conductivity, a strong drift field will need to build up in the bulk to sustain the discharge current[72], which can be noticed in the electric field distribution in figure 5(d). And with the radius of dust particle increasing from 80 nm to 100 nm, the drift field heating effect is more pronounced, compared with the reversed field heating. Similar enhanced

drift field heating has been observed experimentally in a capacitive hydrogen diluted silane discharge in which the amount of dust and negative ions is increased[55]. In fact, the drift field in the bulk depends on the electron density and the collision frequency. Low electron density and high collision frequency may effectively reduce plasma conductivity, and thus enhance the drift heating effect[72]. The enhanced electric field in the bulk would increase the ionization rate to compensate for the electron loss by dust and maintain the global balance of electrons. In addition, as shown in figure 5, the reversed field is weakened at the presence of large dust particles (100 nm) in plasma. This implies that the depletion of electrons and ions by dust may reduce the effect of charge separation during sheath collapse.

The heating mechanism also largely depends on external parameters, such as the power supply frequency, voltage and gas pressure. Figure 6 displays the spatiotemporal evolutions of the electron impact source term (first column) and electric field (second column) at the discharge frequency of 13.56 MHz instead of 50 MHz for different radii of dust particle. The other conditions are the same as in figure 1. We can observe that the typical α-mode heating is weaker than the reversed field heating in the case of 13.56 MHz with the dust particle radius at 1nm, as shown in figure 6(a) and 6(b). In fact, as the frequency decreases, the sheath oscillation frequency slows down, resulting in a decrease in α-mode heating during the expansion phase. Accordingly, the reversed field heating becomes relatively apparent. On the other hand, with the radius of dust particle at 100 nm, the drift field heating gradually dominates the electron heating, and the valid discharge area becomes more narrow.

Figure 7 compares spatiotemporal plots of the electron impact source term at the pressure of 300 mTorr (first row), and 100 mTorr (second row), with dust particle radius of 1 nm and 80 nm at the frequency of 50 MHz. As can be seen from figure 7(a), for the case of 1 nm dust particles, the heating mechanism is dominated by α-mode at the pressure of 300 mTorr, accompanied by the local field reversal heating. However, at the lower pressure as shown in figure 7(c), it is hard to observe the field reversal heating, due to the fact that in this case, less collisions would make electrons respond and neutralize the charge separation efficiently during the collapse period. This further implies the dependence of the field reversal on the gas pressure. Besides, for the lower pressure in figure 7(d), the introduction of the large dust particles into the plasma does not have a significant effect on the heating mechanism,

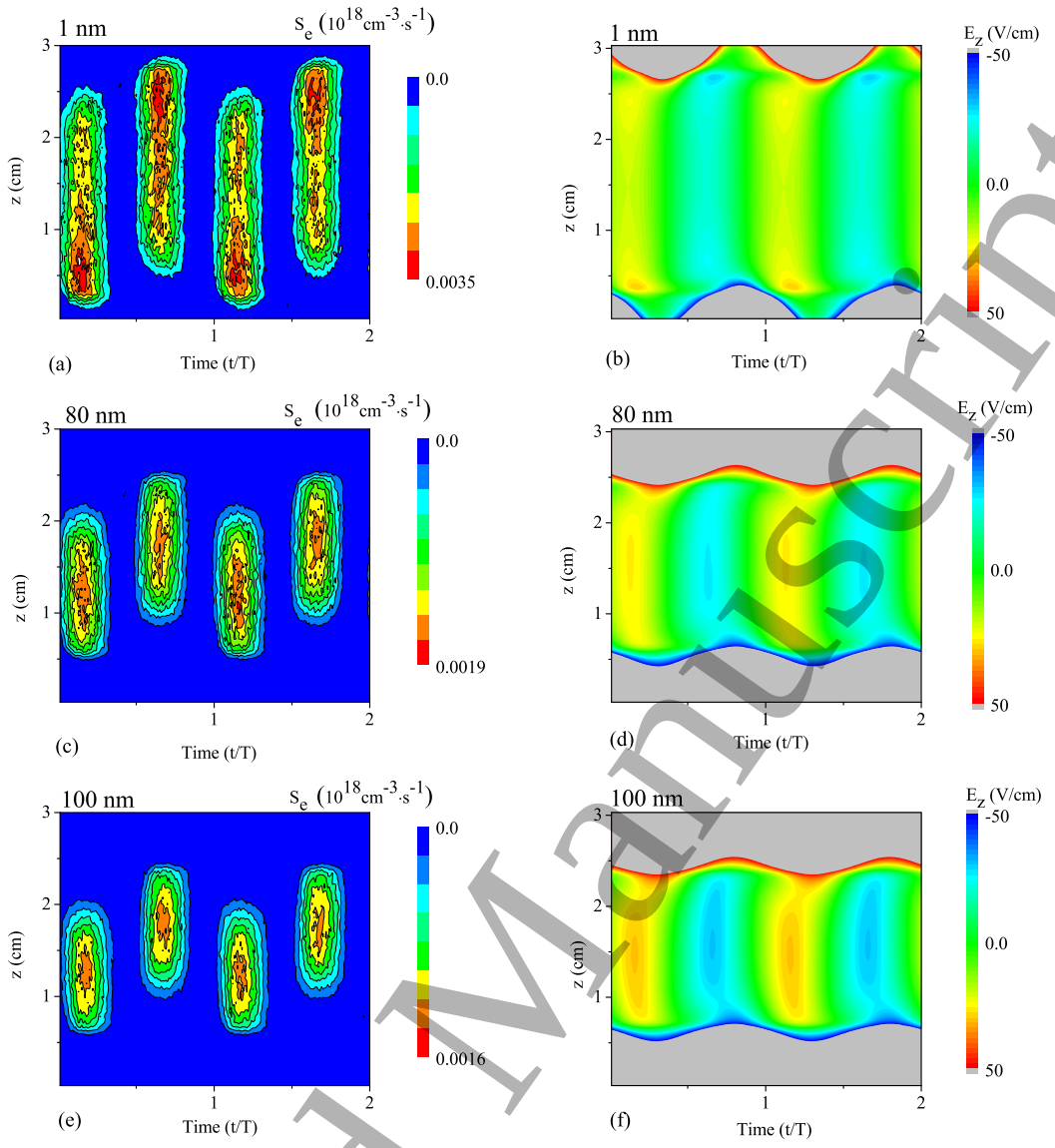

Figure 6. Spatiotemporal evolutions of electron impact source term(first column), corresponding electric field (second column) during two rf cycles in SiH_4 discharges driven by 13.56 MHz, for dust radius of 1 nm (first row), 80 nm (second row), 100 nm (third row) present in the plasma. Other discharge conditions are same as in figure 1

but produces a thicker sheath due to a decrease in plasma density.

Subsequently, figure 8 shows spatiotemporal plots of the electron impact source term at the voltage of 100 V (first row), and 140 V(second row), with dust particle radius of 1 nm and 80 nm at the frequency of 50 MHz. For the voltage of 140 V, similar results of the electron impact source term are obtained compared with those in the lower voltage case

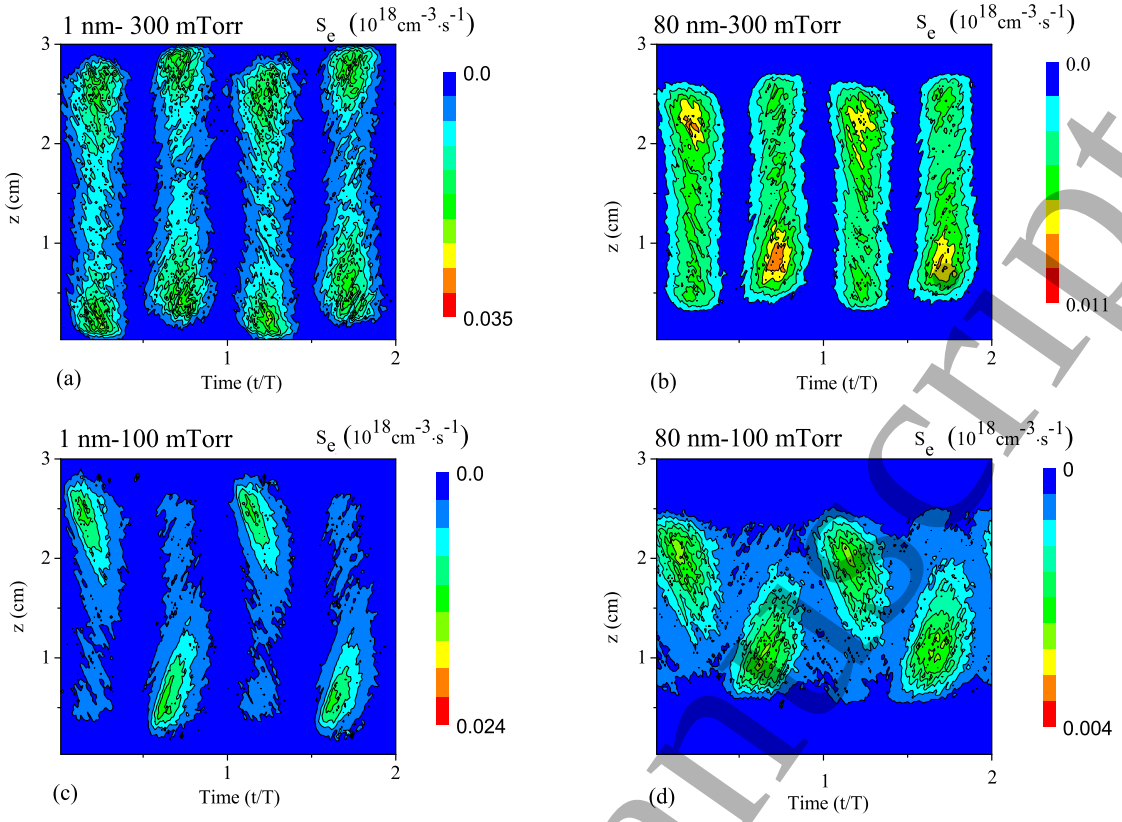

Figure 7. Spatiotemporal evolutions of electron impact source term at the pressure of 300 mTorr (first row, as reference case), and 100 mTorr (second row), in SiH_4 discharges driven by 50 MHz, for dust radius of 1 nm (first column) and 80 nm (second column) present in the plasma. Other discharge conditions are same as in figure 1

except much higher values. Actually, the α–mode and reversed field heating are enhanced due to the increased sheath voltage drop at a higher RF voltage, resulting in larger electron impact source during either sheath expansion or sheath collapse.

3.3 Distributions of the dust particles

In this section, we mainly focus on the spatial distribution of dust particles. Generally, for small dust particles, the distribution which satisfies the parabolic distribution between the electrodes is similar to that of the negative ion due to relatively small ion drag force acting on them. For large dust particles, greater ion drag force makes them move toward the electrodes, while the electric field force near the sheath has the opposite effect. And then,

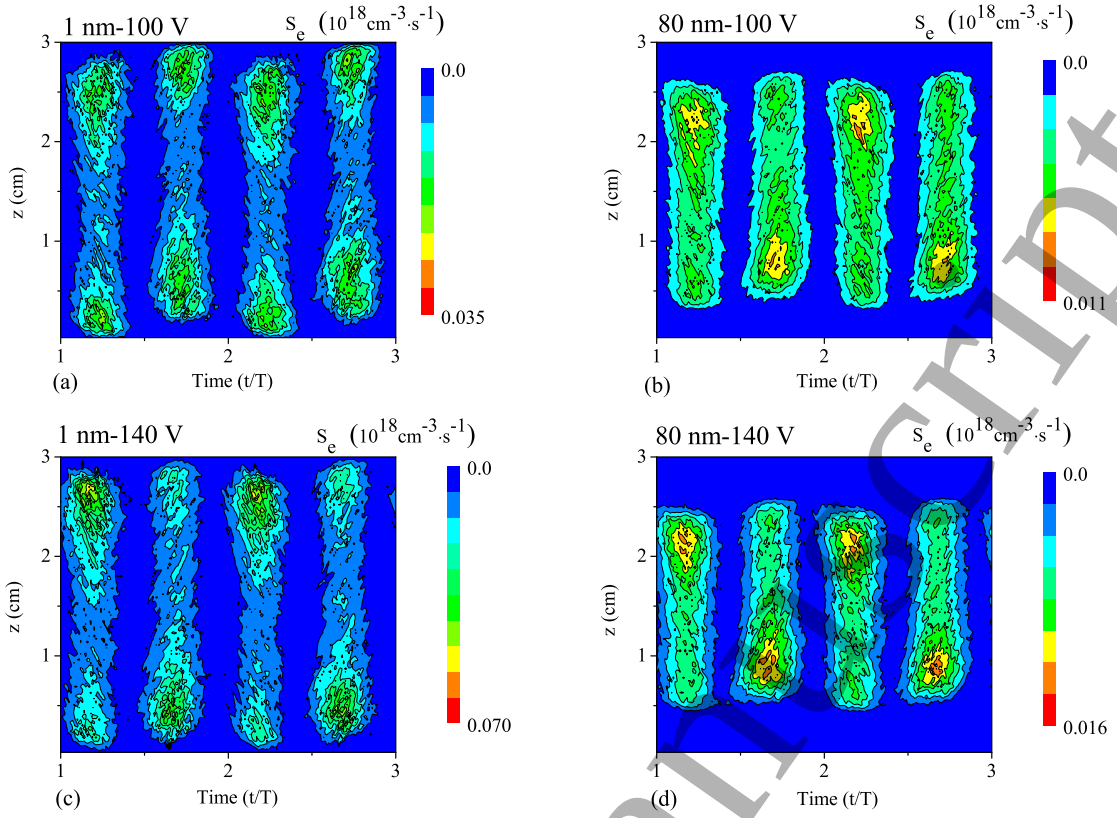

Figure 8. Spatiotemporal evolutions of electron impact source term at the voltage of 100 V (first row, as reference case) and 140 V (second row) in SiH_4 discharges driven by 50 MHz, for dust radius of 1 nm (first column) and 80 nm (second column) present in the plasma. Other discharge conditions are same as in figure 1

stable peaks in the density profiles will be established near the sheaths where the electric field force is in equilibrium with the ion drag force[77, 86]. It is reported when two distinct peaks of dust density appear near the sheaths with very few particles left in the discharge center, a typical so-called void phenomenon will be formed[7, 63, 87, 88].

Figure 9 shows the profiles of time averaged dust density, electrical field force and ion drag force acting on the dust particle for different particle sizes at the base conditions. It is found in our simulation that, the distribution of dust particles with radius of 1 nm tends to form a small bimodal structure with a relatively small value located in the discharge center and two peaks also in the bulk, indicating that the effect of the ion drag force can not be ignored here. For dust particles with radius larger than 1nm, their distributions are typically two peak structures, as expected[40, 43, 46, 63]. On the other hand, as the dust

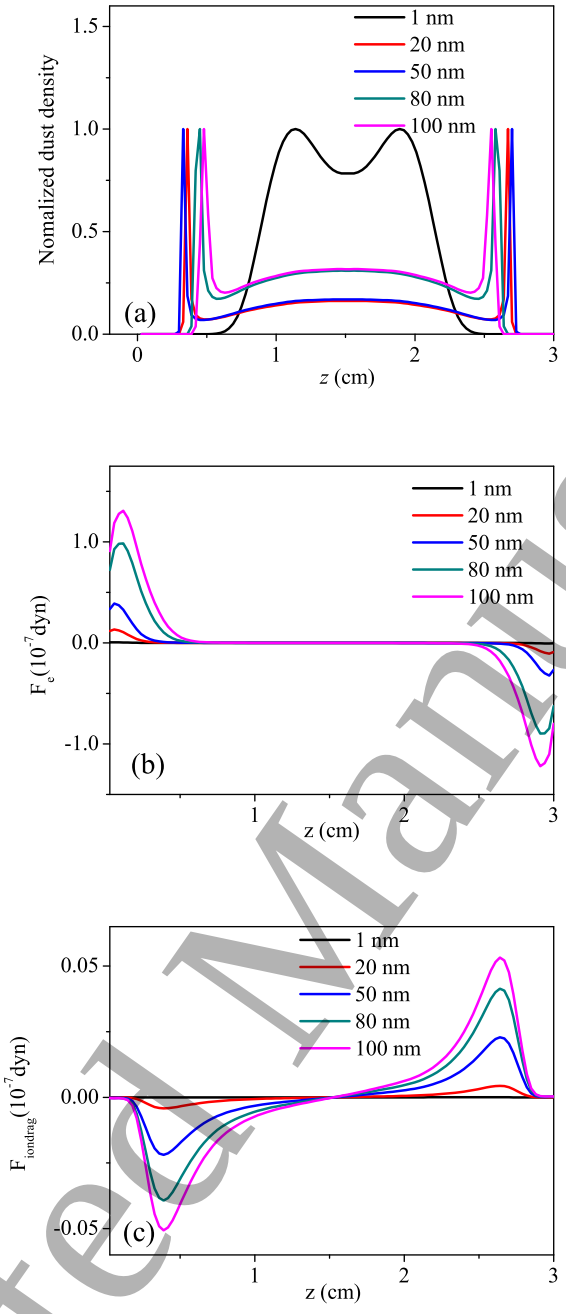

Figure 9. The profiles of time-averaged dust density (a), electric field force (b) and ion drag force (c) acting on the dust, for different particle sizes at the base discharge conditions. The dust density is normalized with the corresponding maximum value in order to compare the change of the dust peak. The discharge conditions are same as in figure 1.

particle radius changes from 1 nm to 50 nm, the peaks tend to move toward the electrodes, mainly due to the increasing ion drag force compared with the electrical field force, as shown in figure 9(b) and (c). At the same time, the sheath thickness does not change greatly as shown in figure 2(d). However, when the radius of dust particle changes from 50 nm to 80 nm or even 100 nm, the sheath thickness begins to widen due to great electron loss, so that the peaks move back toward the bulk.

It has been noticed when the voltage amplitude is reduced[87] or the pressure is increased[88], the dust void tends to disappear. But, up to now, little work has been done on the effect of the external parameters on the dust bimodal structure. To get a deeper insights, we first display in figure 10, with the radius of dust particle fixed at 50 nm, the axial distribution of time averaged dust density, electron density, electric field, as well as corresponding electric field force and ion drag force acting on the dust particles, for different gas pressure. Compared with the case of 100 mTorr, the sheath thickness decreases at 300 mTorr as seen from figure 10(b), causing the peaks to move toward the electrodes as seen from figure 10(a). In addition, with increasing pressure, the peak values of the electric field force in the sheath increase, while those of the ion drag force are reduced. In general, the ion drag force depends on the positive ion flux Γ_i and the χ in equation 4. For pressure of 300 mTorr, although the ion flux at the peak position of the ion drag force increases from 4.7 $\times 10^{14}$ to 11×10^{14} $\mathrm{cm^{-2}s^{-1}}$, a slower transport process (leading to a lower mean velocity of the ion ν_s) and a smaller electron Debye length (leading to a lower coulomb logarithm coefficient) would be obtained due to an increased dissipation of the electron energy in inelastic collisions, leading to the decreasing maximum value of χ from 6.9×10^{-24} to 2.1×10^{-24} ($\mathrm{g\cdot cm\cdot s^{-1}}$). As a result, these factors induce an decrease in ion drag forces.

For the case of different voltages, the corresponding profiles are shown in figure 11, with the dust particle radius of 50 nm. It is obvious that for a higher voltage of 140 V the dust peaks move toward the bulk compared with the case of 100 V, which is still attributed to a larger sheath thickness. And with the increase of voltage, both the peak values of the electric field force and ion drag force increase, as shown in figure 11(c). As for a larger ion drag force at higher voltage, it is attributed to the increase of ion flux from 11×10^{14} to 14×10^{14} $\mathrm{cm^{-2}s^{-1}}$ and the change in χ value from 2.1×10^{-24} to 3.2×10^{-24} ($\mathrm{g\cdot cm\cdot s^{-1}}$)

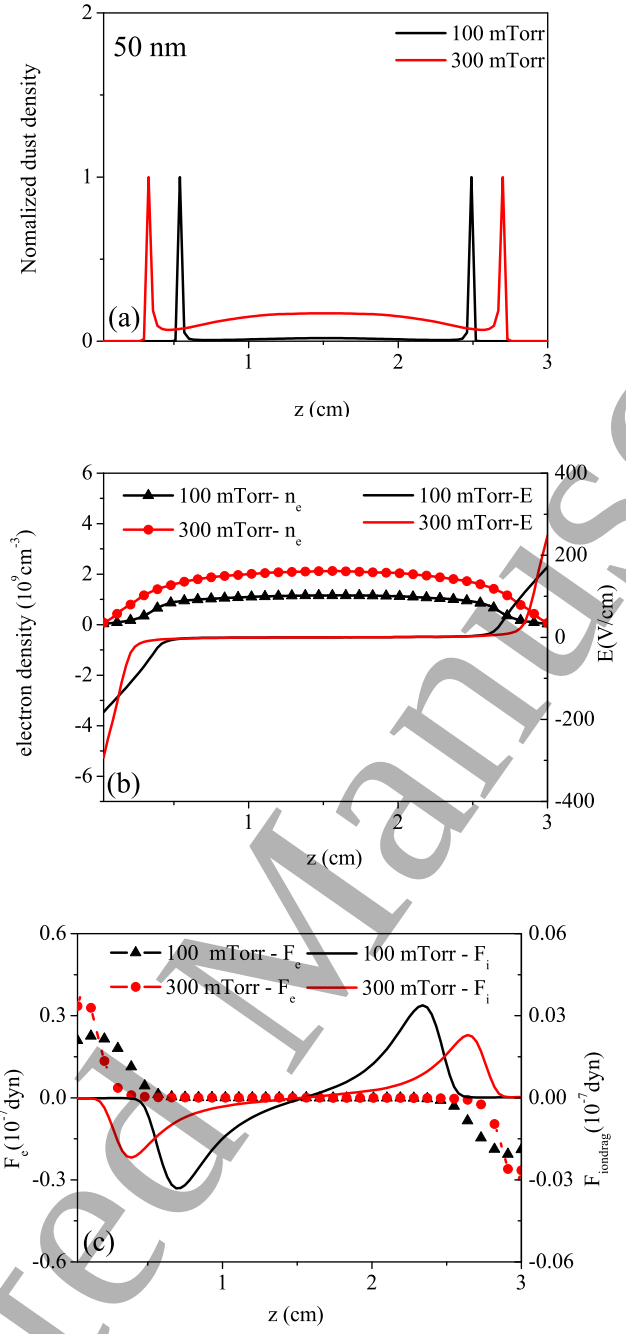

Figure 10. The profiles of time-averaged dust density (a), electron density and electric field (b), and corresponding electric field force and ion drag force acting on the dust (c), for different pressure. Other discharge conditions are same as in figure 1. The dust density is normalized by the corresponding maximum value in order to compare the change of the dust peak.

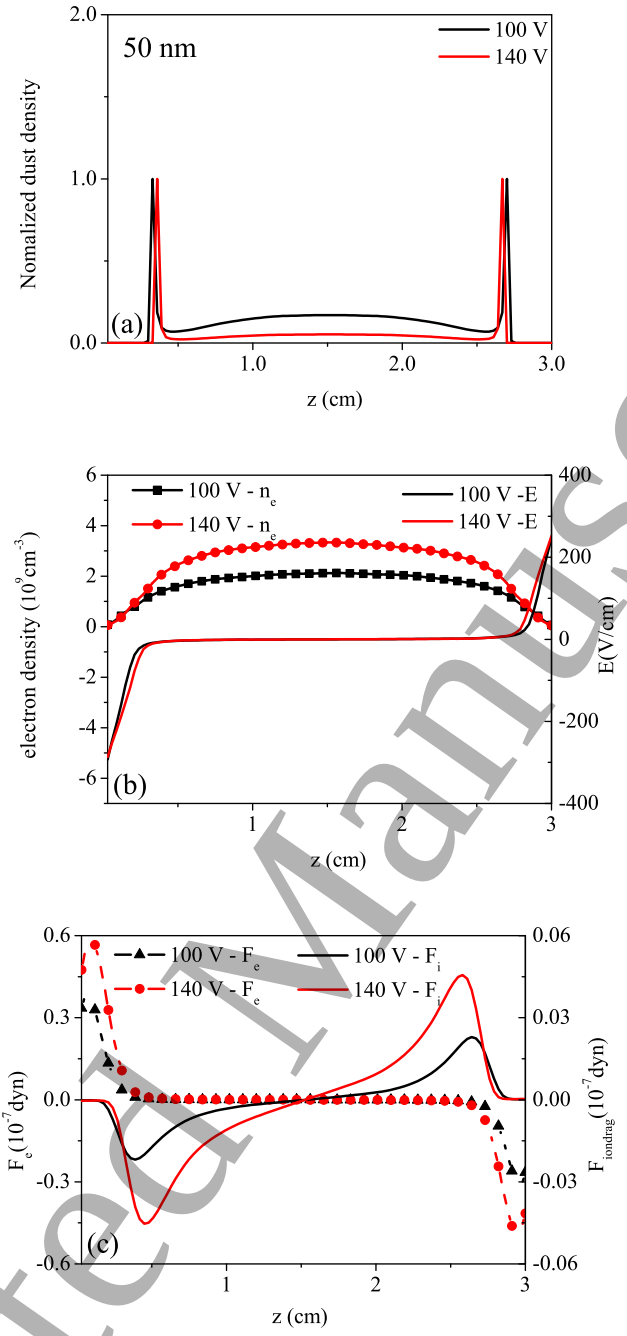

Figure 11. The profiles of time-averaged dust density (a), electron density and electric field (b), and corresponding electric field force and ion drag force acting on the dust (c), for different voltages. Other discharge conditions are same as in figure 1. The dust density is normalized by the corresponding maximum value in order to compare the change of the dust peak.

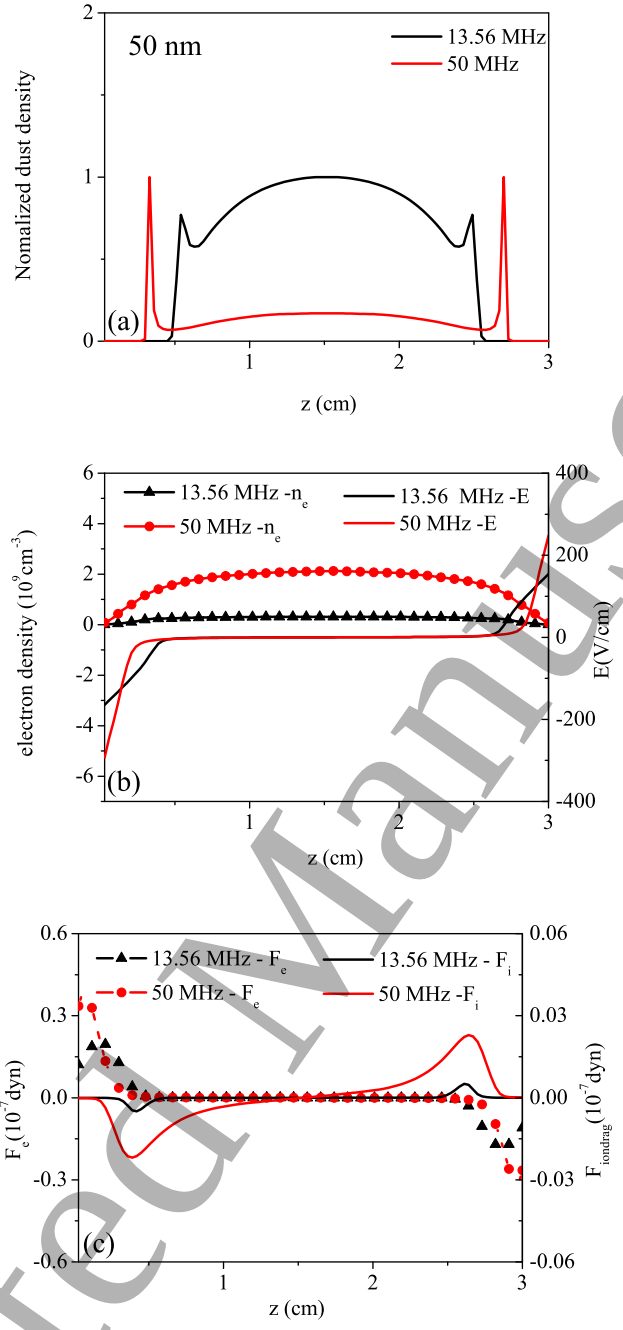

Figure 12. The profiles of time-averaged dust density (a), electron density and electric field (b), and corresponding electric field force and ion drag force acting on the dust (c), for different driving frequencies. Other discharge conditions are same as in figure 1. The dust density is normalized by the corresponding maximum value in order to compare the change of the dust peak.

at the peak position of the ion drag force. In fact, the increase in the value of χ, to a large extent, depends on the increase in ion mean velocity under high voltage conditions. For different operating RF frequencies, almost the same profiles are exhibited in figure 12. In the case of higher RF of 50 MHz, the dramatic increase of the peak value of ion drag force mainly depends on the ion flux increase from 1.6 $\times 10^{14}$ to 11×10^{14} $cm^{-2}s^{-1}$, although the value of χ decreases from 3.11×10^{-24} to 2.11×10^{-24}($g \cdot cm \cdot s^{-1}$). In addition, except for the above analysis of the change trend of the ion drag force, for the electric field force, the above simulation results show that the electric field force increases with the increase of the pressure, voltage and frequency, which is attributed to two factors. On the one hand, because of higher pressure, frequency and voltage operating condition, dust will collect more electrons. On the other hand, the corresponding electric field in the sheath also increases.

4 CONCLUSION

In this work, a 1D hybrid fluid/MC model has been developed to study the effect of different sizes of dust particle on the plasma properties in a pure silane discharge, especially for the plasma density, electron temperature, sheath properties, EEDF and the heating mechanism. The simulations reveal that when the dust particles are relatively small, even with their radii less than 50nm, the changes in plasma properties are not quite significant. Once the radius of dust particle reaches 80 nm or 100 nm, the electron density decreases due to the recombination on the dust surface, accompanied by an increase in electron temperature to maintain the discharge. In particular, evident overshoots are observed in time evolution profiles of positive and negative ion densities, due to the sudden increase in electron temperature. And then, subsequent decreases in the ion density appear due to the decrease in the generation source caused by dust. Finally, a steady state of the plasma is obtained.

For silane plasma without dust particles, a hybrid combination of α-mode and local field reversal heating is present at the base conditions, in which the decrease in the pressure, as well as the driving voltage and frequency, may weaken the reversed field heating. However, by increasing the dust particle radius in the plasma, the drift field heating is enhanced gradually and dominates the heating mechanism, which is mainly due to the consumption of electrons by the dust particles, resulting in a low electrical conductivity, and consequently

an enhanced drift field in the bulk.

In addition, the axial distribution of the dust particles in the plasma easily forms a bimodal structure. Moreover, with the increase in the radius of the dust particle, the two peaks first move towards the electrodes as a result of the increasing ion drag force, and then move away from the electrodes due to the increase of sheath thickness caused by a lower electron density. Furthermore, the effect of external discharge parameters including the pressure, voltage and frequency on the bimodal structure has been well investigated. Finally, in the next study, we will investigate dust void and vortex formation by a two-dimensional fluid/MC model self-consistently coupled with an aerosol dynamics model in which the dust growth process will be taken into account.

Acknowledgements

This work was supported by the National Natural Science Foundation of China (Grant No. 11675036, 11705017 and 11275038), the Fundamental Research Funds for the Central Universities (Grant No. DUT17LK51) and the European Marie Skłodowska-Curie Individual Fellowship within H2020 (Grant Agreement 702604)

References:

[1] Melzer A, Nunomura S, Samsonov D and Goree J 2000 Phys. Rev. E. 62 4162

[2] Nunomura S, Goree J, Hu J S, Wang X and Bhattacharjee A 2002 Phys. Rev. E. 65 1

[3] Ivlev A. V, Steinberg V, Kompaneets R, Hofner H, Sidorenko I and Morfill G. E 2007 Phys. Rev. Lett. 98 145003

[4] Khrapak S A, Morfill G E, Ivlev A V, Thomas H M, Beysens D A, Zappoli B, Fortov V E, Lipaev A M and Molotkov V I 2006 Phys. Rev. Lett. 96 015001

[5] Sütterlin K R, Wysocki A, Ivlev A V, Räth C, Thomas H M, Rubin-Zuzic M, Goedheer W J, Fortov V E, Lipaev A M, Molotkov V I, Petrov O F, Morfill G E and Löwen H, 2009 Phys. Rev. Lett. 102 085003

[6] Chai K B and Bellan P M 2016 Physics of Plasmas. 23 023701

[7] Morfill G E, Thomas H M, Konopka U, Rothermel H, Zuzic M, Ivlev A and Goree J, 1999 Phys. Rev. Lett. 83 1598

[8] Dahiya R P, Paeva G V, Stoffels W W, Stoffels E, Kroesen G M W, Avinash K and Bhattacharjee A, 2002 Phys. Rev. Lett. 89 125001

[9] Veprek S, Reiprich S and Shizi L, 1995 Appl. Phys. Lett. 66 2640

[10] Ostrikov K, 2005 Rev. Mod. Phys. 77, 489

[11] Cabarrocas P R i, Morral A F i and Poissant Y, 2002 Thin Solid Films. 403 39

[12] Poissant Y, Chatterjee P and Cabarrocas P R i, 2003 J. Appl. Phys. 94 7305

[13] Hollenstein C, 2000 Plasma physics and controlled fusion, 42 R93

[14] Choi S J, and Kushner M J, 1993 J. Appl. Phys. 74 853

[15] Howling A A, Sansonnens L, Dorier J L and Hollenstein C, 1993 J. Phys. D: Appl. Phys. 26 1003

[16] Vepřek S, Schopper K, Ambacher O, Rieger W and Vepřek Heijman M G J, 1993 J. Electrochem. Soc. 140 1935

[17] Kawasaki H, Ohkura H, Fukuzawa T, Shiratani M, Watanabe Y, Yamamoto Y, Suganuma S, Hori M and Goto T, 1997 Jpn. J. Appi. Phys. 36 4985

[18] Swihart M T and Girshick S L, 1999 J. Phys. Chem. B. 103 64

[19] Bhandarkar U V, Swihart M T, Girshick S L and Kortshagen U R, 2000 J. Phys. D: Appl. Phys. 33 2731

[20] Gallagher A, Howling A and Hollenstein C, 2002 J. Appl. Phys. 91, 5571

[21] De Bleecker K, Bogaerts A and Goedheer W, 2006 Phys. Rev. E. 73 026405

[22] Deschenaux C, Affolter A, Magni D, Hollenstein C and Fayet P, 1999 J. Phys. D: Appl. Phys. 32 1876

[23] Hong S, Berndt J and Winter J, 2003 Plasma Sources Sci. Technol. 12 46

[24] Benedikt J, Consoli A, Schulze M and von Keudell A, 2007 J. Phys. Chem. A. 111 10453

[25] Mao M and Bogaerts A, 2010 J. Phys. D: Appl. Phys. 43 205201

[26] Mao M, Benedikt J, Consoli A and A. Bogaerts, 2008 J. Phys. D: Appl. Phys. 41 225201

[27] Gallagher A, 2000 Phys. Rev. E. 62 2690

[28] Bhandarkar U V, Swihart M T, Girshick S L and Kortshagen U R, 2000 J. Phys. D: Appl. Phys. 33 2731

[29] Watanabe Y, Shiratani M, Fukuzawa T, Kawasaki H, Ueda Y, Singh S and Ohkura H, 1996 J. Vac. Sci. Technol. A. 14 995

[30] Fukuzawa T, Obata K, Kawasaki H, Shiratani M and Watanabe Y, 1996 J. Appl. Phys. 80

3202

[31] Watanabe Y, 1994 Plasma Phys. Control. Fusion, vol. 39 A59

[32] Boufendi L and Bouchoule A, 1994 Plasma Sources Sci. Technol. 3 262

[33] Watanabe Y, 2006 J. Phys. D: Appl. Phys. 39 R329

[34] Kim K S and Kim D J, 2000 Journal of Applied Physics. 87 2691

[35] Shiratani M, Kawasaki H, Fukuzawa T, Yoshioka T, Ueda Y, Singh S and Watanabe Y, 1996 J. Appl. Phys. 79 104

[36] Kim K S, Kim D J, Yoon J H, Park J Y, Watanabe Y and Shiratani M, 2003 Journal of colloid and interface science. 257 195

[37] Mankelevich Y A, Olevanov M A and Rakhimova T V, 2008 Plasma Sources Sci. Technol. 17 015013

[38] Kim Y, Kim H U, Shin Y, Kang S and Kim T, 2014 Journal of Mechanical Science and Technology. 28 4693

[39] De Bleecker K, Bogaerts A, Gijbels R and Goedheer W, 2004 Phys. Rev. E 69 056409

[40] De Bleecker K, Bogaerts A and Goedheer W, 2006 New J. Phys. 8 178

[41] Allen J E, Annaratone B M and De Angelis U, 2000 J. Plasma. Phys. 63 299

[42] Warthesen S J and Girshick S L, 2007 Plasma Chemistry and Plasma Processing. 27 292

[43] Rozsa K, Bano G and Gallagher A, 2001 IEEE transactions on plasma science. 29 256

[44] Ravi L and Girshick S L, 2009 Phys. Rev. E. 79 026408

[45] Agarwal P and Girshick S L, 2012 Plasma Sources Sci. Technol. 21 055023

[46] Agarwal P and Girshick S L, 2014 Plasma Chem Plasma Process. 34 489

[47] Akdim M R and Goedheer W J, 2001 Physical Review E. 65 015401

[48] Sommerer T J, Barnes M S, Keller J H, McCaughey M J and Kushner M J, 1991 Appl. Phys. Lett. 59 638

[49] Bouchoule A and Boufendi L, 1994 Plasma Sources Sci. Technol. 3 292

[50] Akdim M R and Goedheer W J, 2003 Phys. Rev. E 67 066407

[51] Klindworth M, Arp O and Piel A, 2007 Rev. Sci. Instrum. 78 033502

[52] Hübner S and Melzer A, 2009 Phys. Rev. Lett. 102 215001

[53] Melzer A, Hübner S, Lewerentz L, Matyash K, Schneider R and Ikkurthi R, 2011 Phys. Rev. E 83 036411

[54] Killer C, Bandelow G, Matyash K, Schneider R and Melzer A, 2013 Phys. Plasmas 20 083704

[55] Schüngel E, Mohr S, Iwashita S, Schulze J and Czarnetzki U, 2013 J. Phys. D: Appl. Phys. 46 175205

[56] Bilik N, Anthony R, Merritt B A, Aydil E S and Kortshagen U R, 2015 J. Phys. D: Appl. Phys. 48 105204

[57] Samsonov D and Goree J, 1999 Phys. Rev. E 59 1047

[58] Schülze M, von Keudell A and Awakowicz P, 2006 Plasma Sources Sci. Technol. 15 556

[59] Land V and Goedheer W J, 2007 New J. Phys. 9 246

[60] Killer C, Wegner T, Melzer A and Meichsner J, 2015 Plasma Phys. 22 123702

[61] McCaughey M J and Kushner M J, 1991 J. Appl. Phys. 69 6952

[62] Deka M K, Bailung H and Adhikary N C, 2013 Chin. Phys. B 22 045201

[63] Goedheer W J, Akdim M R and Chutov Yu I, 2004 Contrib. Plasma Phys. 44 395

[64] Schweigert I V, Alexandrov A L and Ariskin D A, 2014 Plasma Chem Plasma Process. 34 671

[65] Schweigert I V, 2008 Phys. Rev. E. 78 026410

[66] Liu Y X, Zhang Q Z, Liu J, Song Y H, Bogaerts A and Wang Y N, 2012 Appl. Phys. Lett. 101 114101

[67] Liu Y X, Zhang Q Z, Liu J, Song Y H, Bogaerts A and Wang Y N, 2013 Plasma Sources Sci. Technol.22 025012

[68] Yan M, Bogaerts A, Goedheer W J and Gijbels R, 2000 Plasma Sources Sci. Technol. 9 583

[69] Yan M, Bogaerts A, Gijbels R and Goedheer W J, 2000 J. Appl. Phys. 87 3628

[70] Gogolides E and Sawin H H, 1992 J. Appl. Phys. 72 3971

[71] Liu G H, Liu Y X, Wen D Q and Wang Y N, 2015 Plasma Sources Sci. Technol. 24 034006

[72] Schülze J, Derzsi A, Dittmann K, Hemke T, Meichsner J and Donko Z, 2011 Phys. Rev. Lett. 107 275001

[73] Mohr S, Schungel E, Schulze J and Czarnetzki U, 2013 J. Phys. D: Appl. Phys. 46 435201

[74] Schülze J, Donko Z, Derzsi A, Korolov I and Schuengel E, 2015 Plasma Sources Sci. Technol. 24 015019

[75] Bohm C and Perrin J, 1991 J. Phys. D: Appl. Phys. 24 865

[76] Boeuf J P and Belenguer P H, 1992 J. Appl. Phys. 71 4751

[77] Akdim M R and Goedheer W J, 2003 J. Appl. Phys. 94 104

[78] Vasenkov A V and Kushner M J, 2002 Phys. Rev. E. 66 066411

[79] Alexandrov A L, Schweigert I V and Peeters F M, 2008 New J. Phys. 10 093025

[80] Mott-Smith H M and Langmuir I, 1926 Phys. Rev. 28 727

[81] Boeuf J P and Punset C, 1999 John Wiley & Sons Inc

[82] Lieberman M A and Lichtenberg A J, Principles of Plasma Discharges and Materials Processing 2nd edn (New York: Wiley, 2005)

[83] De Bleecker K, "Modeling of the formation and behavior of nanoparticles in dusty plasmas". Ph. D. dissertation (Universiteit Antwerpen, 2006)

[84] Nienhuis G J, Goedheer W J, Hamers E A G, van Sark W G J H M and Bezemer J, 1997 J. Appl. Phys. 82 2060

[85] Bouchoule A and Boufendi L, 1993 Plasma Sources Sci. Technol. 2 204

[86] De Bleecker K, Bogaerts A and W. Goedheer, 2004 Phys. Rev. E. 70 056407

[87] Lipaev A M, Khrapak S A, Molotkov V I, Morfill G E, Fortov V E, Ivlev A V, Thomas H M, Khrapak A G, Naumkin V N, Ivanov A I, Tretschev S E and Padalka G I, 2007 Phys. Rev. Lett. 98 265006

[88] Goedheer W J, Land V and Venema J, 2009 J. Phys. D: Appl. Phys. 42 194015

[89] Khrapak S A, Ivlev A V, Morfill G E and Thomas H M, 2002 Phys. Rev. E. 66 046414

[90] Land V and Goedheer W J, 2006 New J. Phys. 8 8